Available online at www.sciencedirect.com
SCIENCE DIRECT®
Ecological Modelling 191 (2006) 83–95
ECOLOGICAL MODELLING
www.elsevier.com/locate/ecolmodel

Habitat mapping using machine learning-extended kernel-based reclassification of an Ikonos satellite image

Andrej Kobler [a,*], Sašo Džeroski [b], Iphigenia Keramitsoglou [c]

[a] *Department of Forest Inventory and Spatial Information Systems, Slovenian Forestry Institute, Vecna pot 2, SI-1000 Ljubljana, Slovenia*
[b] *Department of Knowledge Technologies, Jozef Stefan Institute, Jamova 39, SI-1000 Ljubljana, Slovenia*
[c] *Remote Sensing and Image Processing Team, Department of Applied Physics, University of Athens, Panepistimioupolis, Build PHYS-V, Athens 15784, Greece*

Available online 30 September 2005

Abstract

The spatial resolution of satellite imagery suitable for earth resources studies has improved from 80 m (Landsat-MSS, launched in 1972) to 0.6 m (QuickBird, launched in 2001). The conventional pixel-based methods developed for medium resolution satellite images are not suitable for classification of very high spatial resolution images, because the spectral responses of particular habitat classes are much more variable. On the other hand, in the original Barnsley–Barr kernel-based reclassification algorithm not only the spectral information of a pixel but also the textural information in the vicinity of the pixel is used when the pixel labeling decision is made. The first step of the kernel reclassification algorithm is to perform an initial classification of the original image. In the second step, the adjacency-event matrices are computed for each pixel according to co-occurrence frequencies of the initial classes in the kernel window. The degree of matching between an adjacency-event matrix corresponding to specific pixel and the set of class-specific template matrices produced during training is the criterion for pixel re-labeling. We extend the original kernel-based reclassification algorithm with a decision tree-based reclassification, simultaneously taking into account the class-specific similarity images, which are a side-product of the original algorithm. The advantage of decision tree-extended approach over the original approach seems to be the ability of the former to consider more input information, thus increasing the Kappa classification accuracy for an Ikonos image of our study area from 0.56 to 0.60, using a nomenclature containing 10 habitat classes.

Keywords: Habitat mapping; Classification; Satellite imagery

1. Introduction

For European environmental policy the implementation of the habitat directive (92/43/EEC), the bird directive (79/409/EEC) and the NATURA2000 network is currently one of the most challenging issues.

* Corresponding author. Tel.: +386 1 2007835; fax: +386 1 2573589.
E-mail address: andrej.kobler@gozdis.si (A. Kobler).

0304-3800/$ – see front matter © 2005 Elsevier B.V. All rights reserved.
doi:10.1016/j.ecolmodel.2005.08.002

Intensification of agriculture, tourism and fragmentation are only a few of the serious threats imposed to natural and semi-natural habitats. In most of the EU member states, conservation of biotopes is a high priority issue in environmental policy, making the need to be able to detect changes in the natural environment increasingly pressing. At the same time, reduced financial resources have raised the awareness of ecologists and conservation biologists for innovative techniques for habitat mapping. A powerful suite of tools and data can now be found in the field of earth observation. The strength of this approach is the spatial and temporal consistency of satellite data as well as cost effectiveness. Moreover, it is the only practical way to obtain data from regions difficult to be accessed (e.g., areas with steep topography).

The spatial resolution of satellite imagery suitable for earth resources studies has improved from 80 m (Landsat-MSS, launched in 1972) to 0.6 m (QuickBird, launched in 2001), i.e., more than 10,000 times by area, during a quarter of a century. The need of remote sensing community for very high spatial resolution images (VHSR; ground sampling distance of sensor smaller than 10 m) has now been satisfied, yet there is a gap in image classification, as conventional pixel-based methods developed for medium to low spatial resolution images (e.g., maximum likelihood classifiers; Richards and Jia, 1999) do not seem to be suitable for VHSR images. In VHSR images, the spectral responses of particular habitat classes are much more variable as being composed of the spectral responses of individual class elements (intra-class variability). This results in the 'scene-noise' problem.

The need to take into account not only the spectral information of a pixel (pixel-based classifiers) but also the textural information in the vicinity of the pixel has led to the development of pixel window-based classifiers. A pixel window can be of any size, however, odd-sized squares are used. The labeling decision is made for the central pixel based on the texture (Haralick et al., 1973) or other statistical measures used for spatial feature extraction (Gong et al., 1992). Pixel windows are often referred to as 'kernels'.

Kernel-based reclassification (KRC) software is based on Barnsely and Barr (1996). The kernel reclassification algorithm derives information on land use classes in two stages. The first step is to perform an initial supervised or unsupervised classification to the original image. The number of initial classes varies between specific sites, but 6–12 classes are normally sufficient. In the second stage, the pixel labels are grouped into discrete land use (or habitat) classes on the basis of their frequency of co-occurrence and spatial arrangement within a specified square kernel. The overall classification accuracy reported until now in the literature varies from 74% (Kontoes et al., 2000) to 96% (Barnsely and Barr, 1996) using a two-date multispectral set of IRS-1C LISS-III and Pan, and a single multispectral SPOT-1 HRV image, respectively. It is important to note that both studies address urban environment. Recently, Keramitsoglou et al. (2003) have investigated the potential of projecting this technique to the classification of very high spatial resolution satellite imagery of natural ecosystems. The method was tested on an IKONOS image of Lake Kerkini (Greece), a wetland of great ecological value, included in the NATURA 2000 list of ecosystems. The results show that the algorithm has responded successfully in most cases overcoming problems previously encountered by pixel-based classifiers, such as pixel noise. KRC and object oriented classification were applied to a QuickBird image acquired over Wye Downs National Nature Reserve in UK (Keramitsoglou et al., 2005; Bock et al., 2005). Both methods performed well reaching a correct classification rate of >80% and the performance in individual classes were also good in both methods. The object-oriented method has the advantage of integrating external knowledge which makes the classification of shadowed objects possible, whereas with KRC this cannot be done. On the other hand, KRC gives encouraging results with limited input of external knowledge and is quicker and less labor intensive than the objected oriented method. However, the latter can be applied to large areas irrespective of the existence of large homogenous areas (lacking texture), situations in which KRC fails.

KRC examines labels of adjacent pixels within the square kernel and calculates the so-called adjacency-event matrix (AEM), accounting for the spatial arrangement and frequency of co-occurrence of the labels. Criterion for pixel re-labeling is the degree of matching between an AEM corresponding to specific pixel and the set of class-specific template AEMs produced during training. A side-product of KRC algorithm is thus a set of class-specific similarity images.

The nomenclature used in this study is the European Nature Information System (EUNIS) developed by the European Environment Agency (EEA, 2002). Nomenclatures serve as classification keys that provide the link between ecologically defined habitats and the classes distinguishable on a satellite image (based on spectral values, texture, and/or shape). The EUNIS Habitat classification has been developed to facilitate harmonized description and collection of data across Europe through the use of criteria for habitat identification. It is a comprehensive pan-European system, covering all types of habitats from natural to artificial, from terrestrial to freshwater and marine habitat types. In order to have a meaningful comparison, the two different classifiers were trained using the same set of ground truth data.

The goal of our study was to extend the KRC approach with a machine-learned decision tree-based (DT) reclassification. The DT reclassification uses an additional pre-classified input image based on panchromatic image, and at each pixel reconsiders the whole set of class-specific similarity values in a decision tree, instead of assigning the pixel to the class with the highest similarity value, as in KRC.

2. Data

The study area covers 19.52 km^2 of the most typical habitats in the southwestern part of Slovenia (Fig. 1). It is located within the borders of the proposed Snežnik Regional Park west of Pivka, extending across a spectrum of vegetation successions—from the cultivated alluvial bottom of the Pivka valley (elevation 520 m) eastwards, across the karstic terrain with mostly abandoned pastures and meadows, and up to 880 m elevation on the forested middle slopes of the Javorniki ridge. The study site also includes the dry lakebed of the Palško intermittent karstic lake, one of several such lakes in the region. While this region is considered one of Slovenia's botanical and faunistic biodiversity hot-spots it is also affected by an ongoing process of spontaneous afforestation (SA) of abandoned farmland. This process is the main shaping factor of recent land cover

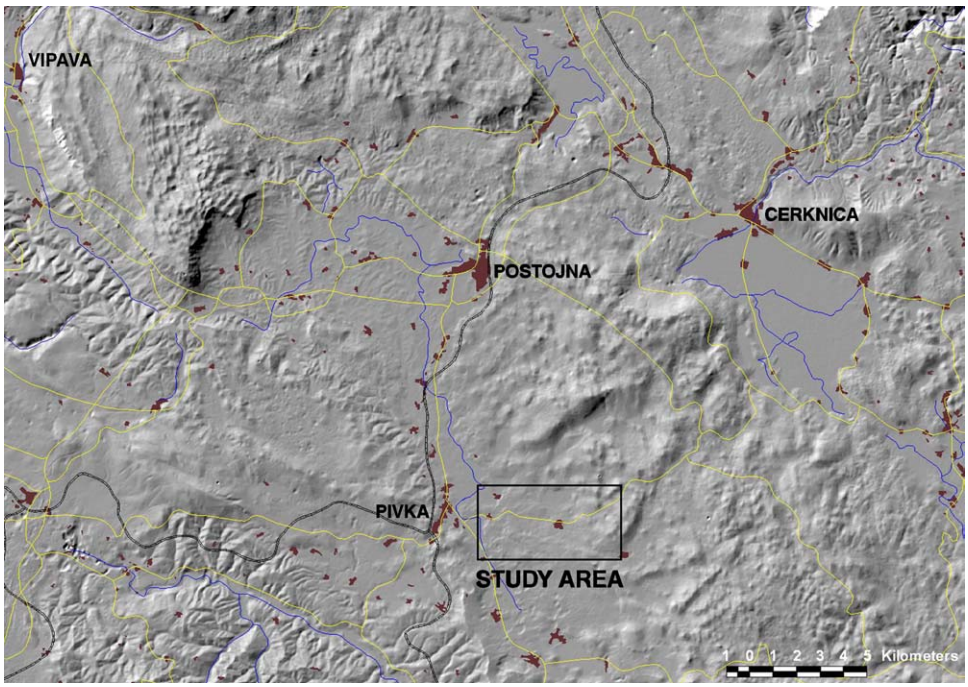

Fig. 1. The location of the study area in vicinity of Pivka, southwestern Slovenia.

Table 1
EUNIS classes found in the study area and used for the final classification

EUNIS code	Description
D5.2	Beds of large sedges normally without free-standing water
E1.5	Mediterraneo-montane grassland
E2.2	Low and medium altitude hay meadows
E3.4	Moist or wet eutrophic and mesotrophic grassland
F3.2	Mediterraneo-montane broadleaved deciduous thickets
F9.2	Willow carr and fen scrub
G1	Broadleaved deciduous woodland
G3	Coniferous woodland
G5.6	Early-stage natural and semi-natural woodlands and regrowth
J	Constructed, industrial and other artificial habitats

change in most of the rural southwestern Slovenia and especially along the eastern rim of the Pivka valley. SA is mainly due to a shift away from agricultural land use but also due to depopulation of marginal areas. It is manifested through a gradual transition from various classes of grassland to a complex patchwork of hedgerows, thickets and forest. The land cover classes found in the study area are listed in Table 1 according to the EUNIS nomenclature.

Our classification is based on an Ikonos 2 satellite image, which has one panchromatic image channel with a 1 m spatial resolution and four multispectral channels (blue, green, red, near infrared) with a 4 m spatial resolution (Fig. 2). The image was acquired on October 14, 2001. The unfavorable image acquisition date probably lowered the accuracy of our classification because of the low sun elevation and long shadows cast by high objects such steep forest edge, and also because of some already defoliated forests in the upper elevations of the study area, causing additional noise in spectral patterns.

The basic ground truth map (Fig. 3) contains 2166 sample polygons covering 10 classes of the EUNIS nomenclature. The map was created by first delineating polygons of homogeneous color and texture from the Ikonos image using segmentation feature of the eCognition tool (www.definiens-imaging.com). Subsequently, the EUNIS classes of the polygons were identified by a combination of field checks and stereoscopic photo-interpretation of aerial imagery. Then a random sample of polygons was selected for each class to create the basic ground truth map. The polygons were rasterized and all the pixels that are closer than 8 m from segment boundaries were rejected in order to mitigate the edge effects with the kernel algorithm. The remaining pixels were randomly sub-sampled with

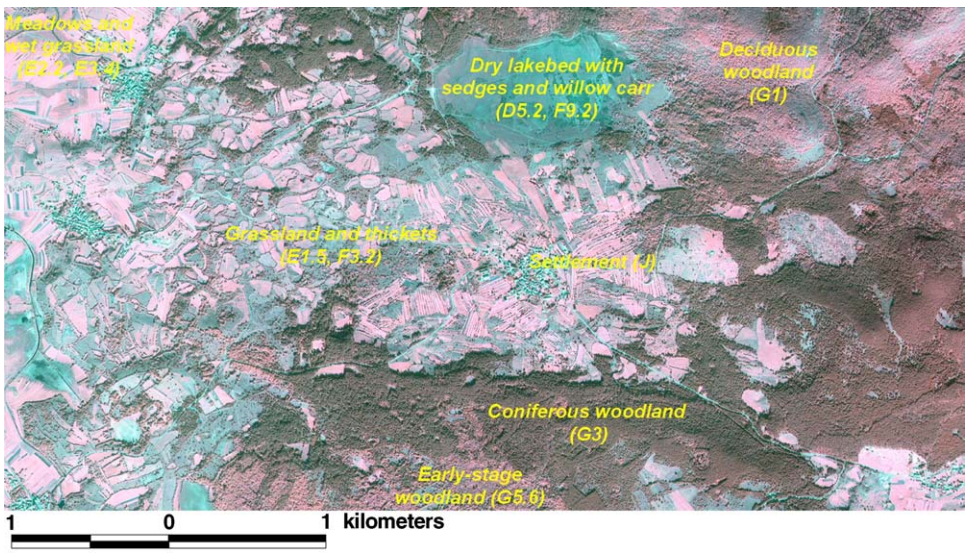

Fig. 2. The Ikonos satellite image of the study area.

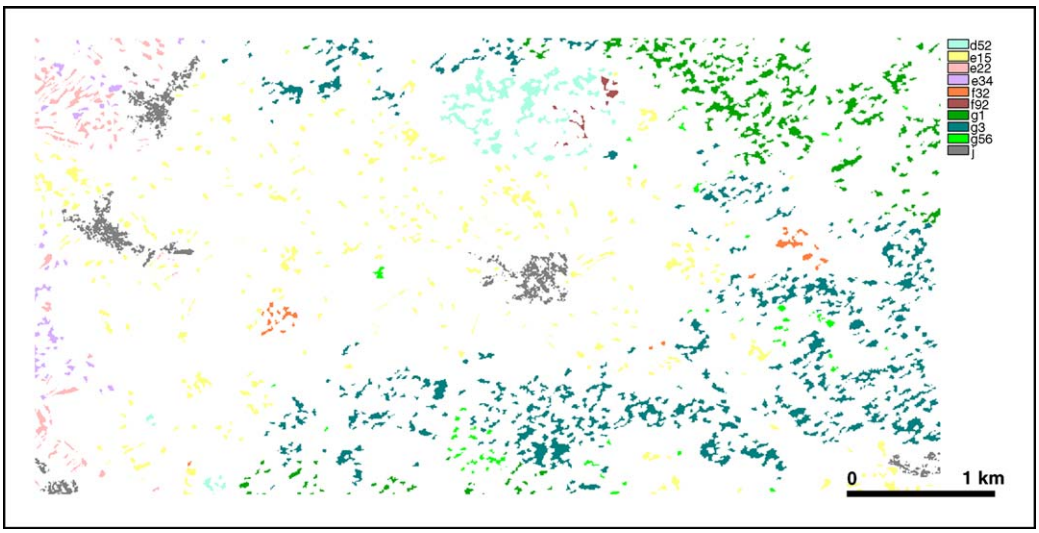

Fig. 3. The basic ground truth map for the study area showing 2166 sample polygons covering 10 classes of the EUNIS nomenclature.

equal representation of classes. Finally, the sampled pixels were distributed into independent reference sets for classification and accuracy estimation, each containing approximately 380 pixels per EUNIS class.

3. Methods

The general setup of our study was as follows (Fig. 4). The input image data were initially pre-

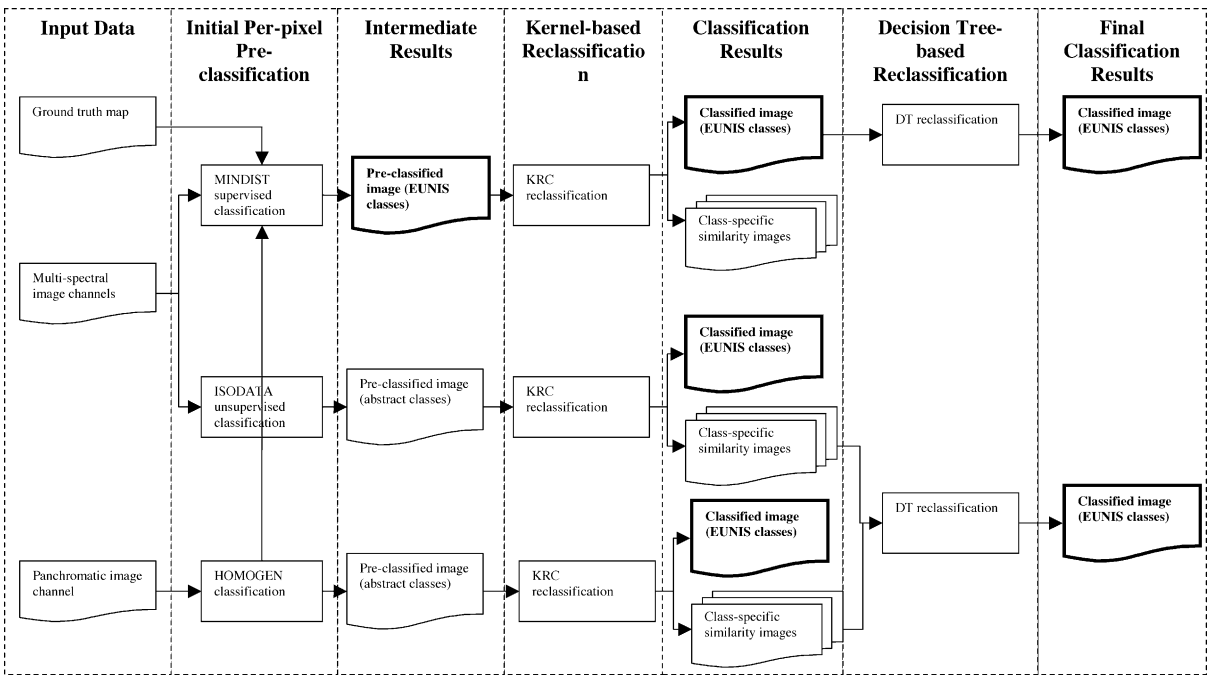

Fig. 4. The flow-chart of the classification. All the kernel-based procedures were performed for kernels 3×3, 5×5, 7×7, and 9×9. Bold frames represent the output maps tested for classification accuracy.

classified using two different per-pixel classification approaches[1]—an unsupervised one, and a supervised one; the latter was used as a baseline approach. Both initial results were then reclassified using KRC. Subsequently, the similarity images as the side-products of the previous KRC runs were used with the decision tree-based classifiers for the final reclassification. All the kernel-based procedures were performed for kernels 3×3, 5×5, 7×7, and 9×9. The data processing (other than image segmentation, minimum-distance-to-means classification, and machine-learning of decision trees) was done using KERNEL.PY tool written in Python.

The original classification algorithm by (Barnsely and Barr, 1996) has two stages—an initial pre-classification, and a subsequent kernel-based reclassification. The input datasets include a very high spatial resolution satellite image and a ground truth map of the same year and season. Using any supervised or unsupervised classification technique we perform an initial pre-classification (on the per-pixel level) of the original image into a nomenclature, which need not be the same as the final output nomenclature (Table 1).

In our study, we comparatively used two initial per-pixel classification approaches. The first one was the unsupervised classification (into 10 abstract classes) of the multispectral channels according to Iterative Self-Organising Data Analysis Technique (ISODATA algorithm; Tou and Gonzales, 1974) until either a 0.95 convergence threshold was achieved or 100 iterations were complete. The second approach was supervised classification using the minimum-distance-to-means (MINDIST) classifier, implemented in IDRISI software (www.clarklabs.org), which assigns an unknown pixel based on its standardized proximity to the nearest class-mean in the image channel space. We used MINDIST to classify multispectral channels and the panchromatic texture homogeneity image into 10 EUNIS classes. The homogeneity image was generated using the homogeneity algorithm by (Haralick et al., 1973) and downsampled to the spatial resolution of the multispectral images (4 m). As the third pre-classified image (HOMOGEN) to be used with KRC we enhanced the homogeneity image using histogram equalization, then we reclassified it into eight discrete classes.

Based on ground truth, template adjacency-event matrices (AEMs) were generated for each EUNIS class from the pre-classified images, by computing a mean AEM from all individual AEMs in a class. An AEM is defined as (Barnsely and Barr, 1996)

$$\mathrm{AEM} = \begin{bmatrix} f_{11} & f_{12} & \dots & f_{1n} \\ f_{21} & f_{22} & \dots & f_{2n} \\ \dots & f_{ij} & \dots & \dots \\ f_{n1} & f_{n2} & \dots & f_{nn} \end{bmatrix}, \quad (1)$$

where f_{ij} is the frequency with which pixels belonging to class i are adjacent to those belonging to class j (i, $j = 1, \dots, n$), within the specified kernel. The size of the square matrix M depends on the number of input classes present in the initially classified image (n). Consider, for example, a 3×3 kernel K with classes A–D and the resulting AEM(K):

$$K = \begin{bmatrix} A & B & B \\ A & C & B \\ A & C & D \end{bmatrix} \quad \Rightarrow$$

$$\mathrm{AEM}(K) = \begin{bmatrix} 4 & 2 & 5 & 0 \\ 2 & 6 & 4 & 1 \\ 5 & 4 & 2 & 2 \\ 0 & 1 & 2 & 0 \end{bmatrix}$$

Next stage of KRC algorithm is the reclassification of the initially classified pixels to the final habitat class which is selected as the one with the highest similarity index value, defined as

$$\Delta_k = 1 - \sqrt{0.5N^{-2} \sum_{i=1}^{C} \sum_{i=j}^{C} (\mathrm{AEM}_{ij} - T_{kij})^2}, \quad (2)$$

where AEM_{ij} is an element of the AEM defined in Eq. (1), T_{kij} the corresponding element for the template AEM of habitat class k, N the total number of adjacency events in the kernel ($N = 20$ for a 3×3 kernel) and C is the number of final habitat classes in the image. From the above it is clear that the values of Δ_k fall in the range between 0 (no similarity) and 1 (perfect match), i.e., $0 \leq \Delta_k \leq 1$.

During the final reclassification stage of KRC we passed a kernel of defined size over the whole pre-

[1] The "per-pixel" denotes a classifier which assigns a pixel according to its feature vector without considering its spatial context, e.g., the surrounding kernel.

classified image and computed the similarity index value between the current and the template AEMs. The KRC algorithm assigns to each pixel the thematic habitat class for which Δ_k is maximum.

For the machine-learning of decision trees we generated two training sets: one with all the similarity index values resulting from KRC run on MINDIST image and another one with similarity index values resulting from KRC runs both on ISODATA and HOMOGEN images. In the latter case, we were thus able to incorporate additional information into the classifier, as compared to the KRC. For each training set and for each kernel size (3×3, 5×5, 7×7, and 9×9) a decision tree combining all the similarity features was generated using a machine-learning tool See5 rel. 1.10 (www.rulequest.com). The decision tree was used for a second-stage reclassification.

Finally, the classification accuracy was estimated for all EUNIS classification results using an independent control sample and the Kappa statistic based on an error matrix. Kappa statistic k (Lillesand and Kiefer, 1994) is conceptually defined as:

$$k = \frac{\text{observed\_accuracy} - \text{chance\_agreement}}{1 - \text{chance\_agreement}}$$

It serves as an indicator of the extent to which the percentage correct values of an error matrix are due to "true" agreement versus "chance" agreement.

4. Results

There were 21 different EUNIS maps generated for the study area. Besides the map generated with the initial MINDIST per-pixel classification, there were three sets of maps generated with KRC from ISODATA, HOMOGEN, and MINDIST pre-classified images, each set containing one map per kernel size ($3 \times 3, \ldots, 9 \times 9$). Further two sets of maps were generated with DT—one from ISODATA- and HOMOGEN-based similarity values and another from MINDIST similarity values. For each KRC-generated map a set of 10 class-specific similarity images were produced to be later used in a DT-based reclassification.

One example of such set of similarity images is given in Fig. 5. By comparing it to the annotated Ikonos image in Fig. 2 we can observe that each class-specific similarity image shows highest values in the areas where there is the focal class present. In some classes the separation between the focal class and the rest is very obvious (e.g., similarity image for class F9.2). However, for some images high similarity values can also be found in areas of non-focal classes. For example, high similarity to class E3.4 (wet grassland) can be found not only in water-saturated depressions but also allover the dry grassland area on higher terrain and also within forests.

Some characteristic EUNIS maps are shown in Fig. 7, and a related decision tree is listed in Fig. 6. A detailed classification accuracy estimation was performed for each map, of which just the overall Kappa values are summarized in Figs. 8 and 9.

From the decision tree given as an example in Fig. 6 it can be seen that not all the similarity images are considered in the tree—note the absence of four criteria based on HOMOGEN (for E1.5, E2.2, F3.2, and G3) and two based on ISODATA (E1.5 and F3.2). Each class is discriminated using two or more criteria, not necessarily including a criterion based on similarity to the actual class being separated. For example, some pixels belonging to class D5.2 were classified using only a combination of similarities to classes G5.6, F9.2, and E3.4.

5. Discussion

As expected, the least accurate EUNIS classification was achieved by the per-pixel classification, which leaves a high level of noise in the result (Fig. 7, upper map). This is due to inability of pixel-based classifiers to consider spatial context which becomes important in very high spatial resolution imagery, when a pixel size falls below the size of objects of interest in the image (e.g., houses, trees). Taking in consideration the spatial context, even using the smallest kernel (3×3), be it with KRC or with DT approach, considerably improves the classification accuracy (Fig. 9). The tradeoff is the loss of spatial detail—note the strong "averaging" effect of a 7×7 kernel in the middle and lower maps in Fig. 7 compared to the upper map in Fig. 7.

Our results for an autumnal Ikonos image of a semi-natural sub-mediterranean landscape show a DT-based reclassification can increase the classification accuracy in comparison to the KRC approach. Looking

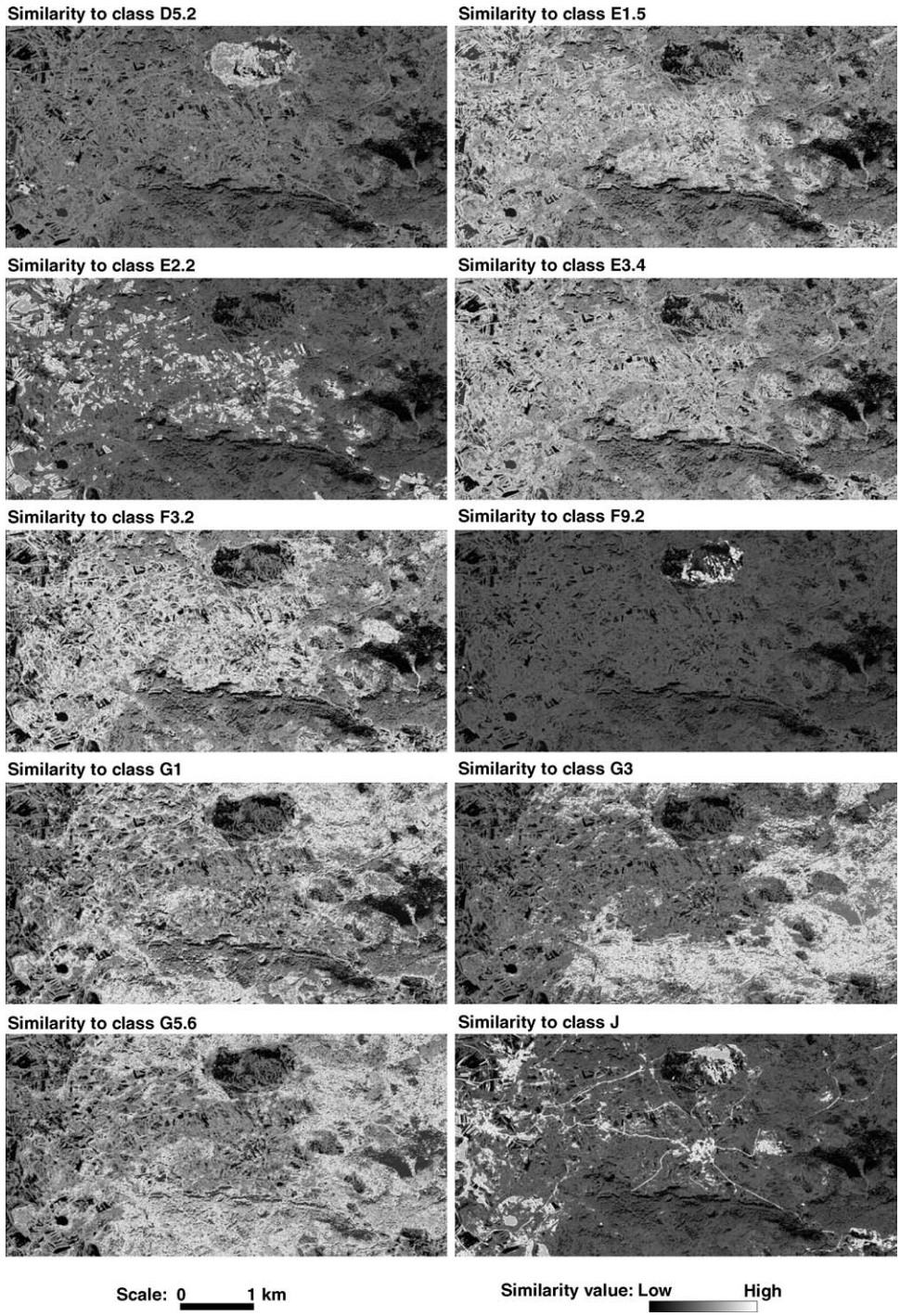

Fig. 5. A side-product from KRC to be used in the machine learning-based reclassification are the sets of class-specific similarity values. Here is an example set generated from the MINDIST pre-classified image using a 7×7 kernel.

```
See5 INDUCTION SYSTEM [Release 1.10] Tue May 25 14:17:00 2004
    Options:
       Pruning confidence level 1%
       Test requires two branches with >= 100 items
Read 3955 cases (21 attributes) from homiso_k7.data
Decision tree:
HOMOGEN_similarity2classG56 <= 0.9233:
:...ISODATA_similarity2classF92 > 0.8721:
:   :...HOMOGEN_similarity2classE34 <= 0.9011: F9.2 (358.0/4.0)
:   :   HOMOGEN_similarity2classE34 > 0.9011: D5.2 (100.0/48.0)
:   ISODATA_similarity2classF92 <= 0.8721:
:   :...ISODATA_similarity2classE22 <= 0.8505:
:       :...ISODATA_similarity2classD52 <= 0.8605: E3.4 (292.0/151.0)
:       :   ISODATA_similarity2classD52 > 0.8605: D5.2 (432.0/122.0)
:       ISODATA_similarity2classE22 > 0.8505:
:       :...HOMOGEN_similarity2classD52 <= 0.8566: E2.2 (241.0/73.0)
:           HOMOGEN_similarity2classD52 > 0.8566:
:           :...HOMOGEN_similarity2classF92 > 0.9142: F3.2 (155.0/92.0)
:               HOMOGEN_similarity2classF92 <= 0.9142:
:               :...ISODATA_similarity2classE34 > 0.9093: E3.4 (134.0/63.0)
:                   ISODATA_similarity2classE34 <= 0.9093:
:                   :...HOMOGEN_similarity2classG56 <= 0.8959: E1.5 (161.0/71.0)
:                       HOMOGEN_similarity2classG56 > 0.8959: E2.2 (100.0/50.0)
HOMOGEN_similarity2classG56 > 0.9233:
:...ISODATA_similarity2classJ > 0.9285: J (397.0/36.0)
    ISODATA_similarity2classJ <= 0.9285:
    :...ISODATA_similarity2classG3 <= 0.9315:
        :...ISODATA_similarity2classG1 > 0.9393: G1 (299.0/85.0)
        :   ISODATA_similarity2classG1 <= 0.9393:
        :   :...ISODATA_similarity2classD52 <= 0.8478: G3 (148.0/100.0)
        :       ISODATA_similarity2classD52 > 0.8478: F3.2 (367.0/94.0)
        ISODATA_similarity2classG3 > 0.9315:
        :...ISODATA_similarity2classG1 > 0.9459:
            :...ISODATA_similarity2classG3 <= 0.9489: G1 (132.0/64.0)
            :   ISODATA_similarity2classG3 > 0.9489: G5.6 (112.0/39.0)
            ISODATA_similarity2classG1 <= 0.9459:
            :...ISODATA_similarity2classG1 <= 0.9165: G3 (103.0/12.0)
                ISODATA_similarity2classG1 > 0.9165:
                :...ISODATA_similarity2classG3 <= 0.9581: G5.6 (101.0/53.0)
                    ISODATA_similarity2classG3 > 0.9581:
                    :...ISODATA_similarity2classD52 <= 0.8584: G3 (111.0/28.0)
                        ISODATA_similarity2classD52 > 0.8584:
                        :...HOMOGEN_similarity2classG1 <= 0.9611: G3 (107.0/47.0)
                            HOMOGEN_similarity2classG1 > 0.9611: G5.6 (105.0/45.0)
```

Fig. 6. An example of a decision tree to reclassify ISODATA- and HOMOGEN-based similarity values (kernel 7×7), generated with the See5 machine learning tool. Note that the lower map in Fig. 7 depicts the classification result of this particular decision tree.

just at one kernel size (Fig. 8), e.g., 7×7, we can see that the least accurate is the kernel-based reclassification of HOMOGEN image (probably because HOMOGEN only describes one of many possible aspects of texture pattern in the panchromatic channel), followed by KRC of ISODATA image. The highest accuracy with a 7×7 kernel size is achieved by DT, which is simultaneously taking into account similarity values related to both HOMOGEN and ISODATA images.

We assume that the added accuracy of DT based on both ISODATA and HOMOGEN pre-classified images is due to its ability to consider more input information than the KRC. This assumption is substantiated by a close overlap of accuracy values between both classification approaches when the same amount of input information is provided (Fig. 9).

It might perhaps look tempting to merge pre-classified ISODATA and HOMOGEN images to maximize information content of the input image before

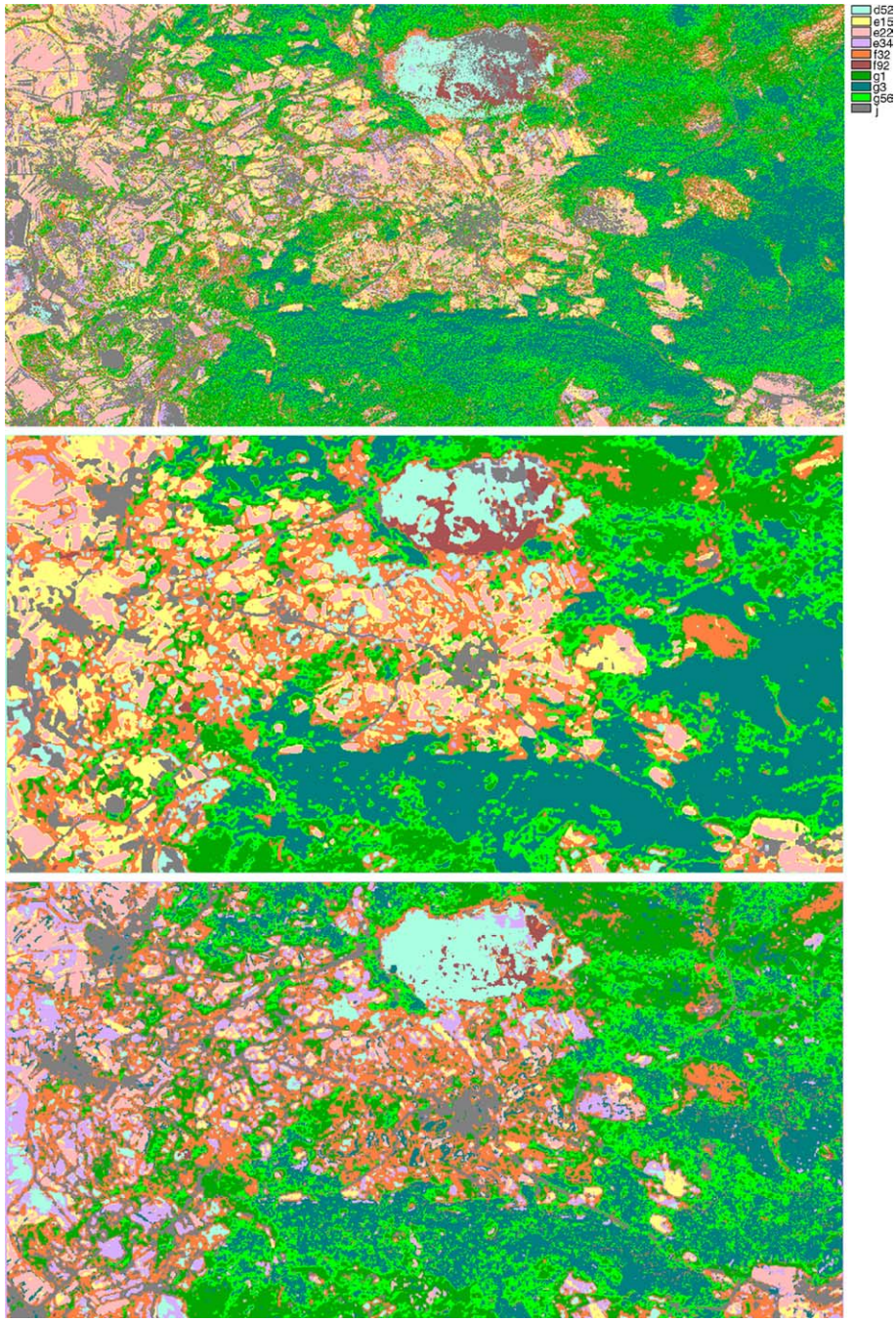

Fig. 7. Typical examples of the generated EUNIS maps; the upper map is the result of the initial per-pixel MINDIST pre-classification, the middle map is the result of the kernel-based reclassification of the ISODATA image using a 7×7 kernel, the lower map is the result of the decision tree-based reclassification of the ISODATA- and HOMOGEN-based similarity images using a 7×7 kernel. Their respective Kappa accuracies are 0.48, 0.56, and 0.60. Note that Fig. 6 shows the decision tree used to produce the lower map.

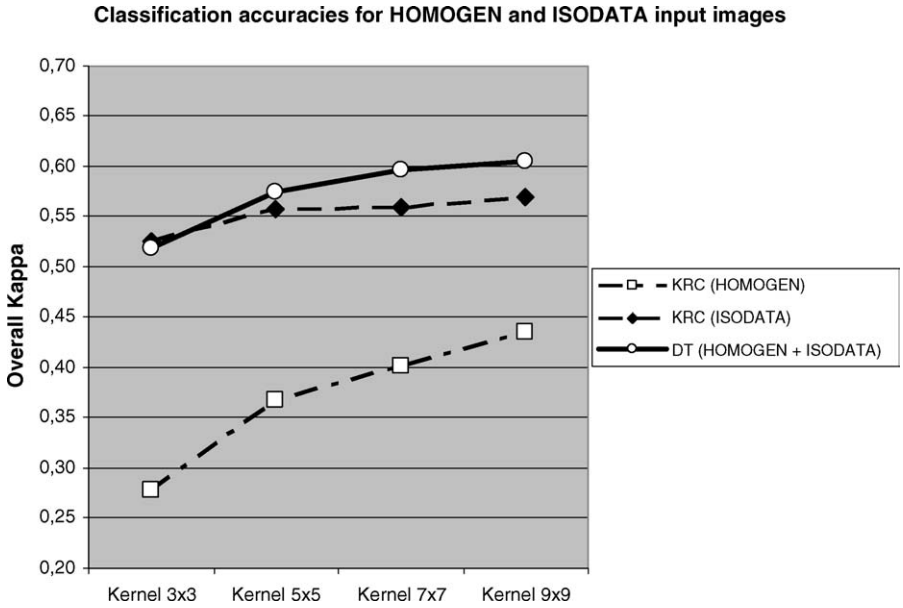

Fig. 8. Comparison of classification accuracies according to kernel size for (1) the kernel-based reclassification of HOMOGEN image (KRC), (2) kernel-based reclassification of ISODATA image, and (3) decision tree reclassification of both HOMOGEN and ISODATA images (DT).

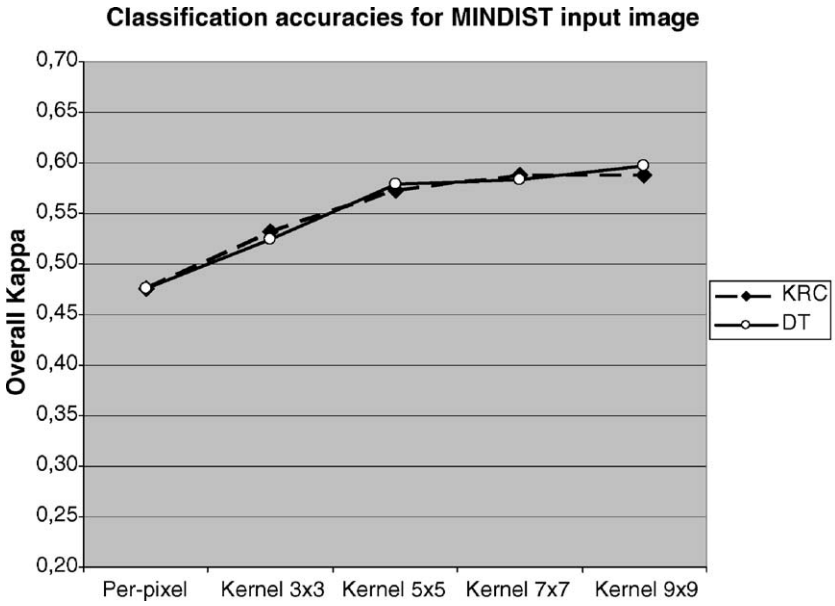

Fig. 9. Comparison of classification accuracies for ISODATA input image according to kernel size for (1) kernel-based reclassification (KRC) and for (2) decision tree reclassification (DT). Note that the per-pixel value on the left indicates the accuracy of the ISODATA pre-classification itself.

applying the KRC. However, using a large n is not reasonable for two reasons. Firstly, in our case 10 classes in ISODATA image by 8 classes in HOMOGEN image would yield $n = 80$ classes in a merged image. A large n yields a large AEM, which is costly to compute. Secondly, a large n yields an AEM with many cells equaling 0, because only a limited number of co-occurrence types can be expected in any kernel. Such an AEM is statistically not very significant.

The main advantage of DT approach over the KRC approach, as detected in this study, is therefore ability of the former to consider more input information. This advantage is achieved without losing the conceptual simplicity or ease of implementation characteristic for the KRC.

To illustrate this advantage, consider that by attributing a pixel to a class just on the basis of the maximum similarity value we get some wetlands also classified as settlements, i.e., class J (observe the dry lakebed and the eastern rim of the middle map in Fig. 7 for KRC and Fig. 2 as the visual reference). By considering and additional criterion (similarity to class G5.6) the DT was able to identify this area as wetlands (Fig. 7, lower map).

Furthermore, our results confirm (Figs. 8 and 9), that using both the KRC and the DT approach, we can improve the accuracy of a per-pixel classification, be it unsupervised, such as ISODATA or HOMOGEN, or supervised, such as MINDIST. It must be kept in mind however, that accuracy of the initial pre-classification affects the success of the reclassification—in other words, error in the first is propagated through to the second, so the accuracy improvement cannot be very substantial. This improvement increases with kernel size, as is obvious from the increasing chart lines in Fig. 8 and especially from Fig. 9, which includes also accuracy value for the initial ISODATA classification. On the other hand, the downside of a larger kernel is a degradation of the effective spatial resolution of the output maps to $(\text{kernel\_size} - 1) \times \text{pixel\_size}$. In the case of 4 m spatial resolution of the input image, and kernel sizes of 3, 5, 7, and 9, this means a deterioration of effective resolutions to 8, 16, 24, and 32 m respectively. Note, for example, the difference in the level of spatial detail between upper map in Fig. 7 (per-pixel classification) and the middle map in Fig. 7 (kernel size 7).

The point of optimal compromise between classification accuracy and spatial resolution depends on the specific needs of the user. The DT approach has a special appeal in this respect, because it enables inclusion of more input information into the classifier. In this way, a better resolution can be retained with a particular level of accuracy, or a better accuracy can be achieved at a particular level of spatial detail.

By comparing one set of similarity images in Fig. 5 to the annotated Ikonos image in Fig. 2 we can observe that each class-specific similarity image does show high values in the areas where there is the focal class present. In some classes, the separation between the focal class and the rest is very obvious (e.g., similarity image for class F9.2). However, for some class-specific similarity images high similarity values can also be found in areas of non-focal classes. For example, high similarity to class E3.4 (wet grassland) can be found not only in water-saturated depressions but also allover the dry grassland area on higher terrain and also within forests. A similar problem with classes E1.5 and F3.2 is reflected by the absence of the related criteria in the decision tree (Fig. 6). In cases like this the DT approach would easily enable us to improve the separation among classes by incorporating additional input datasets into the learning stage and into the reclassification. We could have extended the input dataset with (1) textural measures other than homogeneity (Haralick et al., 1973), (2) multi-date imagery could have been used instead of single-date in order to capture typical phonological patterns, and (3) ancillary thematic GIS layers could have been used, such as digital terrain model or pedological map.

The applicability of KRC algorithm and its transferability to different spatial resolutions and biogeographical regions is another point of interest. Keramitsoglou et al. (2005) have shown that the results of KRC application to QuickBird and IKONOS very high spatial resolution images of different test sites are encouraging. The overall accuracies attained were above 70%, whilst the level of class hierarchy reached ranged from EUNIS level 1 to level 5. It appears that the finer the spatial resolution the better the performance of the classifier. However, the algorithm does not work on images which have coarser resolution and/or exhibit lack of texture. This highlights the constraint of the algorithm

transferability to highly homogeneous regions and/or to the classification of satellite images of spatial resolution less than 10 m.

Acknowledgements

This work was funded by the Spatial Indicators for European Nature Conservation (SPIN) research project supported by the European Commission under the Fifth Framework Programme. Contract no.: EVG 1-CT-2000-019 (project web site: www.spin-project.org). We are thankful to the two anonymous reviewers for their very useful remarks.

References

Barnsely, M.J., Barr, S.L., 1996. Inferring urban land use from satellite sensor images using kernel-based spatial re-classification. Photogrammetric Eng. Remote Sensing 62 (8), 949–958.

Bock, M., Xofis, P., Rossner, G., Wissen, M., Mitchley, J., 2005. Object oriented methods for habitat mapping in multiple scales: case studies from Northern Germany and North Downs, GB. J. Nat. Conserv. 13, 75–90.

EEA, European Environmental Agency, 2002. EUNIS Habitat classification web application. Electronic Source: http://mrw.wallonie.be/dgrne/sibw/EUNIS/home.html.

Gong, P., Marceau, D.J., Howarth, P.J., 1992. A comparison of spatial feature extraction algorithms for land-use classification with SPOT HRV data. Rem. Sens. Environ. 40 (2), 137–151.

Haralick, R.M., Shanmugan, K., Dinstein, I., 1973. Textural features for image classification. IEEE Trans. Syst. Man Cyber. SMC-3 (November (6)), 610–621.

Keramitsoglou, I., Kontoes, C., Sifakis, N., Mitchley, J., Xofis, P., 2005. Kernel based re-classification of earth observation data for fine scale habitat mapping. J. Nat. Conserv. 13, 91–100.

Keramitsoglou, I., Kontoes, H., Elias, P., Sifakis, N., Fitoka, E., Weiers, S., 2003. Kernel-based re-classification algorithm applied on very high spatial resolution satellite imagery of complex ecosystems. In: Proceedings of the 10th International Symposium of Remote Sensing, Remote Sensing for Agriculture, Ecosystems and Hydrology V, vol. 5232, 8–10 September 2003. Barcelona, Spain, pp. 276–283.

Kontoes, C.C., Raptis, V., Lautner, M., Oberstadler, R., 2000. The potential of kernel classification techniques for land use mapping in urban areas using 5 m-spatial resolution IRS-1C imagery. Int. J. Remote Sensing 21 (16), 3145–3151.

Lillesand, T.M., Kiefer, R.W., 1994. Remote Sensing and Image Interpretation. John Wiley & Sons, New York, p. 616.

Richards, J.A., Jia, X., 1999. Remote Sensing Digital Image Analysis: An Introduction, third, revised and enlarged ed. Springer-Verlag, 363 pp.

Tou, J.T., Gonzales, R.C., 1974. Pattern Recognition Principles. Addison-Wesley Publishing Co., Reading, Massachusetts.